



## Microstructure and residual stress of TiN films deposited at low temperature by arc ion plating

Hai-juan MEI<sup>1,2</sup>, Sheng-sheng ZHAO<sup>1</sup>, Wei CHEN<sup>1</sup>, Qi-min WANG<sup>2</sup>, Hai-feng LIANG<sup>3</sup>

1. School of Mechanical and Electrical Engineering, Shenzhen Polytechnic, Shenzhen 518055, China;

2. School of Mechanical and Electrical Engineering, Guangdong University of Technology, Guangzhou 510006, China;

3. Institute of Technology, East China Jiaotong University, Nanchang 330100, China

Received 8 February 2017; accepted 28 April 2017

**Abstract:** The TiN films were deposited on 316L stainless steel substrates at low temperature by arc ion plating. The influences of substrate bias voltage and temperature on microstructure, residual stress and mechanical properties of the films were investigated by EDS, SEM, XRD and nanoindenter tester, respectively. The results showed that the TiN films were highly oriented in (111) orientation with a face-centered cubic structure. With the increase of substrate bias voltage and temperature, the diffraction peak intensity increased sharply with simultaneous peak narrowing, and the small grain sizes increased from 6.2 to 13.8 nm. As the substrate temperature increased from 10 to 300 °C, the residual compressive stress decreased sharply from 10.2 to 7.7 GPa, which caused the hardness to decrease from 33.1 to 30.6 GPa, while the adhesion strength increased sharply from 9.6 to 21 N.

**Key words:** TiN film; arc ion plating; residual stress; low temperature; bias voltage

### 1 Introduction

In the past decades, TiN films have been widely used to improve the lifetime and performance of cutting tools and mechanical components, which is mainly due to the superior hardness and excellent wear resistance [1–5]. Many researchers have studied the TiN films by physical vapor deposition, such as arc ion plating and magnetron sputtering to satisfy the demand for ever-lower process temperatures. Arc ion plating (AIP) is one of the most widely-used physical vapor deposition techniques, and it is characterized by a combination of high deposition rate and high adhesion force, but the co-deposition of macro-particles is the main barrier to obtain the high performance films with smooth surface [6–8].

In addition, the deposition of films on substrates is usually associated with residual stress development, and the residual stress level is mainly determined by the deposition parameters. It is well known that the deposition parameters such as substrate bias voltage, substrate temperature and nitrogen partial pressure, could

modify the microstructure, surface morphology, residual stress and mechanical properties of films [9–12]. Particularly, substrate bias voltage and temperature are essential to modify the microstructure and mechanical properties due to the improvement of ad-atom mobility and ion bombardment effect. The substrate temperature can effectively and directly enhance the ad-atom mobility through the temperature dependent thermal vibration [13,14]. FESSMANN et al [15] observed that the substrate temperature can be decreased to as low as 100 to 15 °C without decreasing the adhesion strength when TiN films are deposited by a cathodic arc plasma, and sometimes even better results could be obtained at lower temperatures. MEDJANI et al [16] found that lower temperature and moderate bias favor the formation of (002) plane parallel to the substrate surface. However, even the influence of substrate bias voltage and temperature has been investigated in details, but the microstructure and residual stress of the film deposited at a temperature as low as 10 °C by arc ion plating are seldom studied. Moreover, the substrate temperature is constantly changing during the process of deposition, but seldom studies have been reported on the control and

measurement of substrate temperature.

In this work, we presented the deposition of TiN films by arc ion plating at a temperature as low as 10 °C. Moreover, the effects of substrate bias voltage and temperature on the microstructure, macro-particles, residual stress and mechanical properties of the films were investigated.

## 2 Experimental

### 2.1 Film deposition

The TiN thin films were deposited on 316L stainless steel substrates by arc ion plating. One Ti target with a purity of 99.99% was installed on the side walls of the chamber. The distance between target and substrate was 250 mm with the surface of the target parallel to the substrate. Two kinds of stainless steels (50 mm × 10 mm × 0.8 mm, 30 mm × 30 mm × 0.8 mm) were selected as substrates for the test of residual stress and mechanical properties. The elastic modulus ( $E$ ) and Poisson ratio ( $\nu$ ) of the stainless steel were 195 GPa and 0.3, respectively. Prior to the deposition, the substrates were ultrasonically cleaned first in metal detergent and then in deionized water for 5 min, respectively. Then, they were blown dry with N<sub>2</sub> and adhered vertically to the substrate holder with facing towards the target shown in Fig. 1. The metal substrate temperature can be discretionarily adjusted between 10 and 500 °C with the temperature control error less than 5 °C through the way of contact conduction, as shown in Fig. 2.

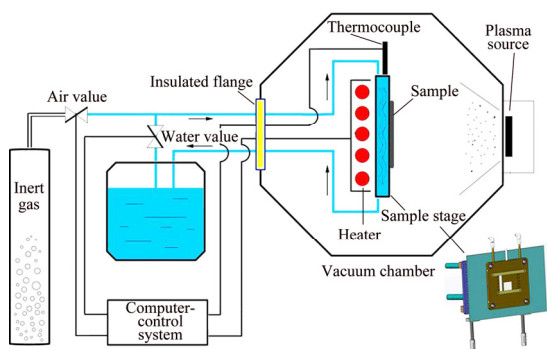


Fig. 1 Metal substrate temperature control device

The chamber was evacuated to a base pressure less than  $5.0 \times 10^{-3}$  Pa, then heated to and kept at a desired temperature by electrical heating or water cooling. To remove surface contaminants, the substrates were plasma-etched by Ar ions for 5 min at a gas pressure of 0.5 Pa and a pulse bias voltage of -800 V with a duty cycle of 40% and frequency of 40 kHz. The deposition took place in an atmosphere of N<sub>2</sub> (99.99% purity) with a working pressure of 1.0 Pa. During the deposition, two series of TiN thin films were deposited at different

substrate bias voltages and substrate temperatures, which are summarized in Table 1. The deposition time was fixed to 30 min to obtain the films with thickness ranging from 1.4 to 1.6 μm.

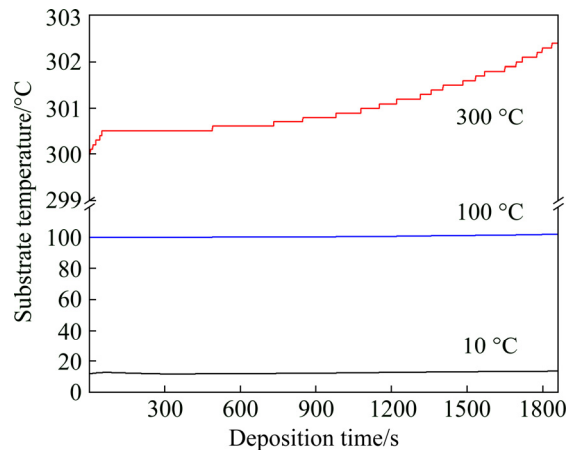


Fig. 2 Substrate temperature as function of deposition time

Table 1 Deposition parameters

Parameter	Value
Base pressure/Pa	$5.0 \times 10^{-3}$
Working pressure/Pa	1.0
Ar flow rate/(mL·min <sup>-1</sup> )	80
N <sub>2</sub> flow rate/(mL·min <sup>-1</sup> )	80
Arc current/A	60
Deposition time/min	30
Target to substrate distance/mm	250
Substrate bias voltage/V	-50, -100, -150, -200
Substrate temperature/°C	10, 100, 300

### 2.2 Film characterization

The surface morphology, thickness and chemical compositions of the films were observed and determined by a scanning electron microscope (FEI, NovaNanoSEM430) equipped with an energy dispersive X-ray spectrum (EDS). The number and size of macroparticles can be automatically counted by the Image-Pro Plus software program [17]. The crystalline structure of the deposited films was identified by X-ray diffraction (Model Bruker D8 Discover) using Cu K<sub>α</sub> radiation under the conditions of 40 kV and 120 mA in  $\theta-2\theta$  geometry.

The residual stress was experimentally measured using film stress tester (FST-1000, Supro Instruments, China) according to substrate curvature method based on the Stoney's equation [18]:

$$\sigma_s = -\frac{E_s}{6(1-\nu_s)} \frac{h_s^2}{h_c} \left( \frac{1}{R} - \frac{1}{R_0} \right) \quad (1)$$

where  $E_s$  and  $\nu_s$  refer to the elastic modulus and Poisson

ratio of substrate, respectively;  $h_s$  and  $h_c$  denote the thicknesses of substrate and film, respectively;  $R_0$  and  $R$  are the curvature radii of the substrate before and after deposition, respectively.

The hardness ( $H$ ) and elastic modulus ( $E$ ) of the films were measured using a nanoindenter (CSM Instrument) with a Berkovich diamond indenter. The indentation depth was kept constantly below 10% of the film thickness to minimize the substrate effect. The adhesion strength was measured by a Micro Scratch-tester (CSM Instrument) using a 200  $\mu\text{m}$ -radius Rockwell C indenter at a maximum load of 30 N, and the scratch length was 3 mm with a scratch speed of 6 mm/min.

### 3 Results and discussion

#### 3.1 Deposition rate and composition

Figure 3 shows the deposition rate of TiN films as a function of substrate bias voltage and temperature. When the substrate bias voltage increased from  $-50$  to  $-100$  V, the deposition rate increased sharply from 2.79 to 3.21  $\mu\text{m}/\text{h}$ , and then decreased to 2.90  $\mu\text{m}/\text{h}$  with further increasing the substrate bias voltage to  $-200$  V. It was consistent with the result that the mobility of ions and the deposition rate increased when the substrate bias voltage was less than  $-100$  V; however, the AIP process was accompanied with the re-sputtering phenomenon at higher substrate bias voltages [19]. Such a change in the deposition rate may be related to two simultaneous effects brought by substrate bias voltage. One is the accelerating deposition effect resulting from the increase of the ion quantity and velocity; the other is the re-sputtering effect due to the ion bombardment. As the substrate temperature increased from 10 to 300  $^\circ\text{C}$ , the deposition rate of TiN films increased sharply from 2.79 to 3.23  $\mu\text{m}/\text{h}$ . At a low substrate temperature, the

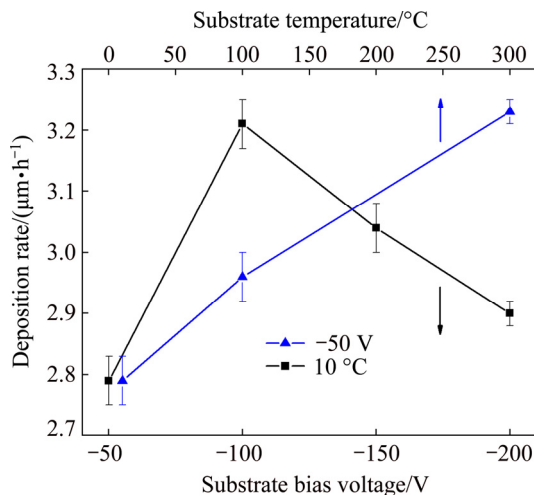


**Fig. 3** Deposition rate of TiN films deposited at different substrate bias voltages and temperatures

small-size islands on the substrate surface could hardly capture the long-range ad-atoms. When the substrate temperature was elevated, which could promote the mobility of ad-atom leading to its accelerated motion along the random directions, the diffusion rate was enhanced and the migrating ad-atoms had a probability to meet and aggregate together [12].

Figure 4 presents the Ti/(Ti+N) mole ratio of TiN films as a function of substrate bias voltage and temperature. It can be seen that the Ti/(Ti+N) mole ratio increased from 0.47 to 0.51 with the increase of substrate bias voltage, which would be due to the combination of ion bombardment mechanism and re-sputtering phenomenon. The rise of substrate bias voltage initiates the re-sputtering of the film, causing a reduction in nitrogen atoms in the film. The enhanced ion bombardment during the deposition process can easily break the weak Ti—N bond and the N atoms are re-sputtered preferentially comparing with Ti atoms [20]. As the substrate temperature increased from 10 to 100  $^\circ\text{C}$ , the Ti/(Ti+N) mole ratio increased slightly from 0.47 to 0.48, but decreased sharply to 0.45 with further increasing the substrate temperature to 300  $^\circ\text{C}$ . It would be due to the upsurge of nitrogen concentration in the deposited film with the increase of substrate temperature [21].

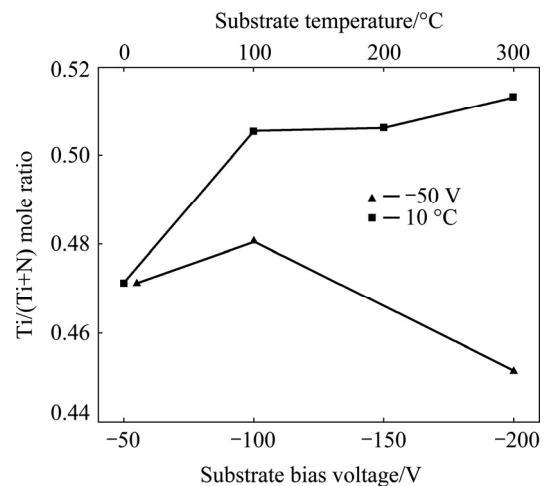
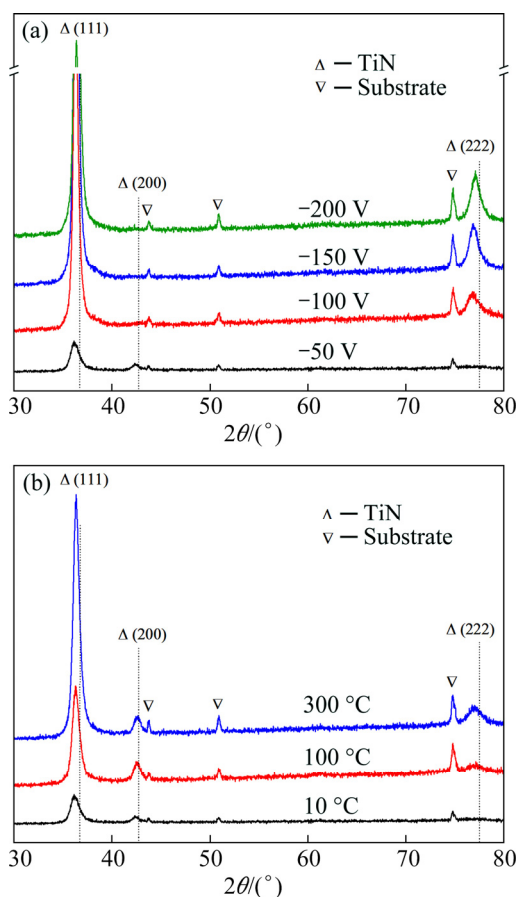


**Fig. 4** Ti/(Ti+N) mole ratio deposited at different substrate bias voltages and temperatures

#### 3.2 Microstructure and morphology

Figure 5 shows the XRD patterns of TiN films deposited at different substrate bias voltages and temperatures. As shown in Fig. 5(a), a slight negative peak shift was observed in XRD patterns of all films, which would be due to the compressive stress in the films. It can be seen that all the TiN films were highly oriented in (111) orientation with a face-centered cubic structure. As the substrate bias voltage increased, the intensity of (111) peak increased sharply as simultaneous

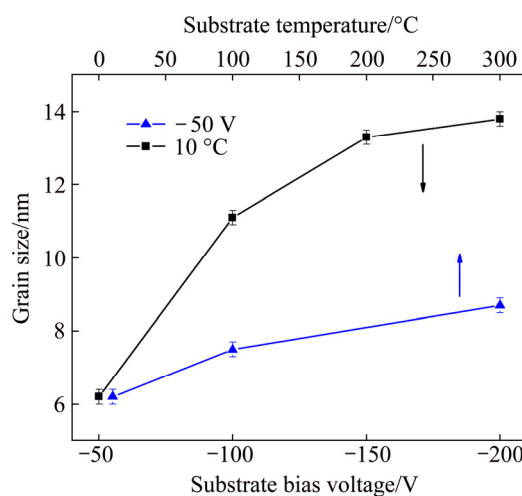
peak narrowing was observed. Moreover, the (200) peak of TiN phase disappeared and the intensity of (222) peak increased gradually when further increasing substrate bias voltage above  $-50$  V. These trends could be explained by the competition between the surface and strain energy [22]. When the strain energy effects ultimately dominate, the TiN films exhibited (111) orientation with the lowest strain energy to minimize the overall energy. Similar trends were found in the XRD patterns of TiN films deposited at different substrate temperatures in Fig. 5(b). When the substrate temperature increased from  $10$  to  $300$  °C, the diffraction peak intensity of TiN films increased gradually and peak narrowing was also observed, which would be due to an indication of either the growth of grain or release of residual stress [23,24]. At higher substrate temperatures, with higher atomic mobility, there was a tendency for epitaxy leading to the nucleation of (111) grains, which resulted in enhancing the crystallization.



**Fig. 5** XRD patterns of TiN films deposited at different substrate bias voltages and same substrate temperature of  $10$  °C (a) and at different substrate temperatures with same substrate bias voltage of  $-50$  V (b)

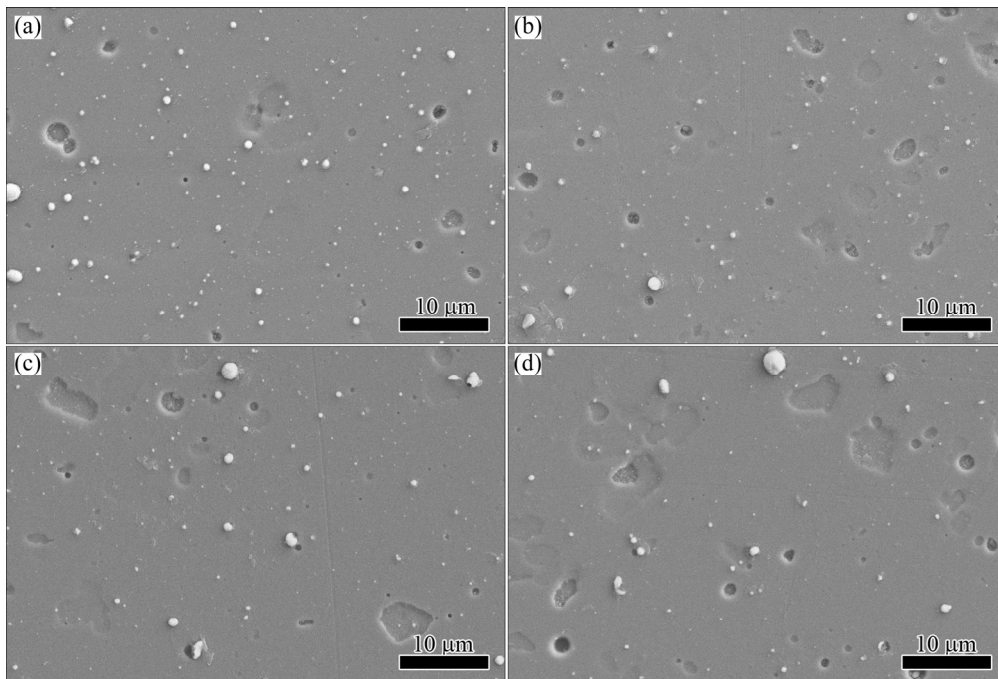
The grain sizes of TiN films deposited at different substrate bias voltages and temperatures shown in Fig. 6 were calculated from TiN (111) peak using Scherrer

formula [25]. As the substrate bias voltage increased from  $-50$  to  $-200$  V, the grain sizes tended to increase sharply from  $6.2$  to  $13.8$  nm, which mainly due to the fact that the effect of ad-atom mobility plays a dominant role in the grain sizes. The film surface achieved high energy delivered by the ions impinging resulting in high atom mobility, which then promoted the migration of particles to the grain boundaries and as a result the grain sizes increased [26]. Meanwhile, the grain sizes of the films increased from  $6.2$  to  $8.7$  nm when the substrate temperature increased from  $10$  to  $300$  °C. However, the effect of substrate temperature on the grain size was less notable when compared with that of substrate bias voltage.

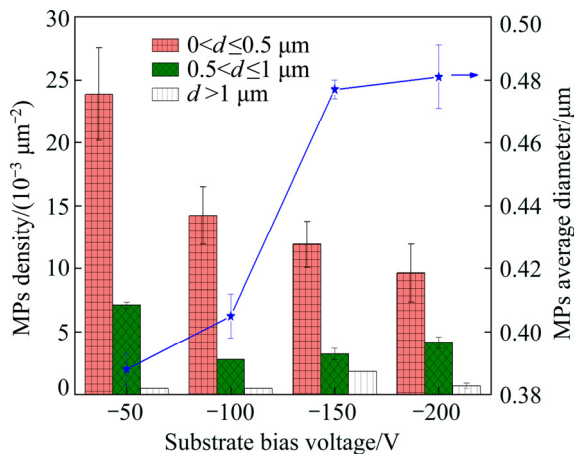


**Fig. 6** Grain sizes of TiN films deposited at different substrate bias voltages and temperatures

Figure 7 shows the surface SEM micrographs of TiN films deposited at various substrate bias voltages. Many macroparticles (MPs) and defects were observed on the film surface, such as the solid droplets, liquid droplets, meshy shallow craters and pinholes, which was a feature of the film deposition by arc ion plating [27]. As the substrate bias voltage increased from  $-50$  to  $-200$  V, the number of MPs reduced gradually and the size of MPs increased. To investigate the distribution of MPs, the number and size of MPs were calculated by the Image-Pro Plus software program. As shown in Fig. 8, most of the MPs diameters concentrated in the range of  $0$  to  $0.5$   $\mu\text{m}$  and the density of MPs decreased gradually as the substrate bias voltage increased from  $-50$  to  $-200$  V. However, the average diameter of MPs increased from  $0.39$  to  $0.48$   $\mu\text{m}$  with the substrate bias voltage increasing, which would be due to the increase of proportion of large size MPs ( $d > 0.5$   $\mu\text{m}$ ). As the substrate bias voltage increased, the ion energy could be so high that after the collision with the ions, some small macro-particles might evaporate before reaching the film surface [28].



**Fig. 7** Surface SEM images of TiN films deposited at substrate temperature of 10 °C and various substrate bias voltages: (a) -50 V; (b) -100 V; (c) -150 V; (d) -200 V



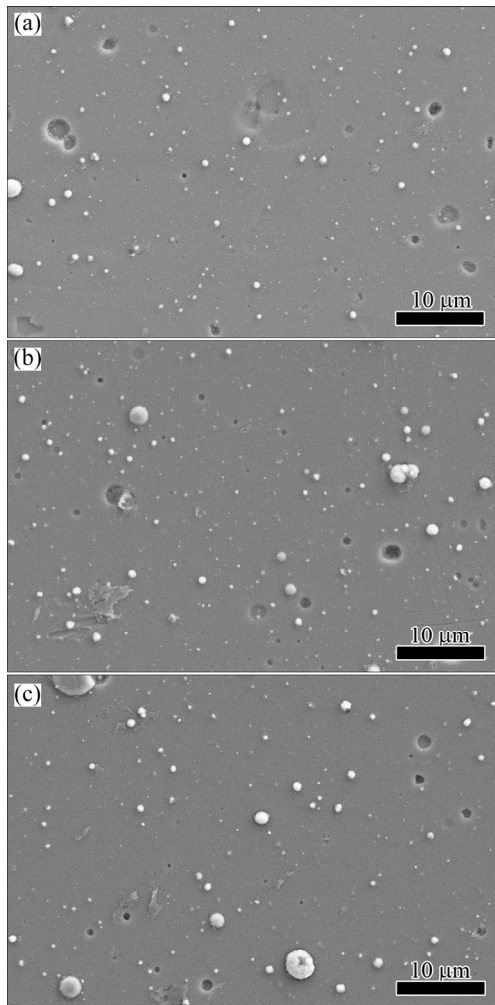
**Fig. 8** Variation in density and average diameter of MPs at various substrate bias voltages

Figure 9 presents the surface SEM images of TiN films deposited at various substrate temperatures from 10 to 300 °C. A slight increase in both the density and the size of MPs with the increase of substrate temperature was consistent with the statistical results, as shown in Fig. 10. It could be seen that most of the MPs diameters concentrated in the range of 0 to 0.5  $\mu\text{m}$  and the density of MPs increased slightly as the substrate temperature increased. Moreover, the average diameter of MPs increased sharply from 0.39 to 0.47  $\mu\text{m}$  initially as the substrate temperature increased from 10 to 100 °C, and then increased slightly to 0.48  $\mu\text{m}$  with further increasing the substrate temperature to 300 °C. At higher substrate

temperatures, with higher surface energy, the contact angle of the droplets attached on the surface becomes smaller, which is beneficial to the adsorption of the liquid droplets on the surface of the coating. Conversely, at low temperatures, the surface energy is low and the droplets are more likely to slip off the surface, especially in the case of high energy ion bombardment.

### 3.3 Residual stress and mechanical properties

The residual stress of TiN films as a function of substrate bias voltage and temperature is shown in Fig. 11. It can be observed that the residual stresses of all the films exhibit a high compressive stress. When the films deposited at a substrate temperature as low as 10 °C, the effect of substrate bias voltage on the residual stress was less notable when compared with that of substrate temperature. The variation of residual stress with different substrate bias voltages and substrate temperatures could be explained by the intrinsic stress and thermal stress [29]. On one hand, the intrinsic stress was dominated by the structure and flaws of the films. The residual compressive stress increased slightly from 10.2 to 10.7 GPa as substrate bias voltage increased from -50 to -150 V, which would be attributed to the following reasons. Firstly, the increase in internal stress was associated with the increased defects raised by the enhanced ion bombardment during the film growth. Secondly, the increased energy of the incident ions was delivered to the growing film when the substrate bias voltage increased, leading to an increase in the internal



**Fig. 9** Surface SEM images of TiN films deposited at substrate bias voltage of  $-50$  V and various substrate temperatures: (a)  $10$  °C; (b)  $100$  °C; (c)  $300$  °C

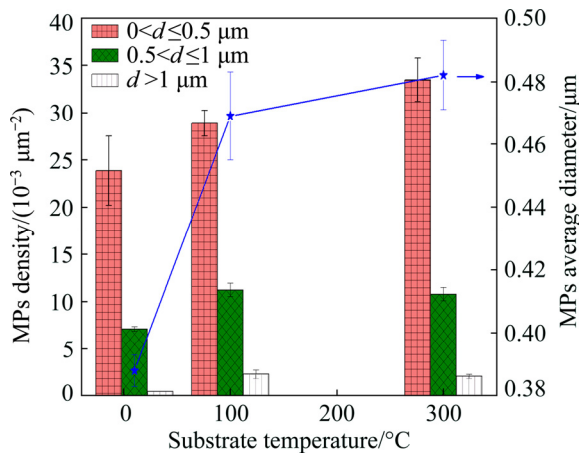


**Fig. 10** Variation in density and average diameter of MPs at various substrate temperatures

stress [30]. With the substrate bias voltage further increasing to  $-200$  V, the higher energy of incident ions delivered to the growing film repaired some defects

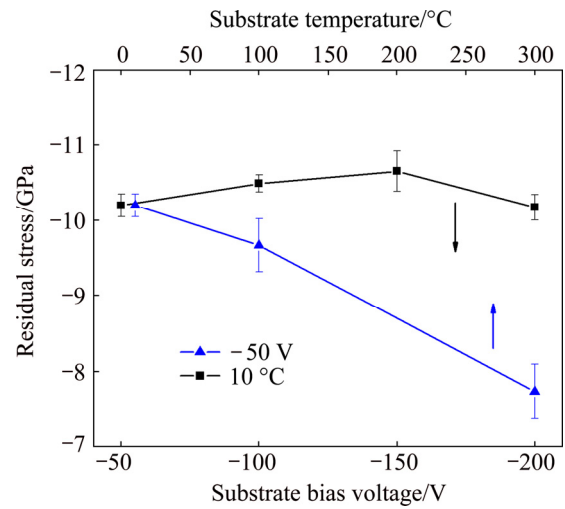


**Fig. 11** Residual stress of TiN films deposited at different substrate bias voltages and temperatures

partly, which could ease the compressive stress at a certain extent. On the other hand, the thermal stress was dominated by the high ratio of substrate temperature ( $T_s$ ) to melting structure of the film material ( $T_m$ ) and the difference coefficient of the thermal expansion between substrate and film ( $\Delta\alpha$ ) [31,32]. When the substrate temperature increased from  $10$  to  $300$  °C, the residual compressive stress decreased sharply from  $10.2$  to  $7.7$  GPa. It could be due to the higher diffusion rate at higher substrate temperatures, which could adjust the misfitted atom to a more equilibrium state and thus relax the intrinsic stress partly. This is similar to the film that the residual compressive stress decreased with the increasing substrate temperature [33]. On the other hand, the decrease in residual compressive stress would be due to the increase of TiN film thickness reported by ZHANG et al [34]. However, in this work, the variation in film thickness is very small ( $1.4$ – $1.6$   $\mu\text{m}$ ), and it can be inferred that the decrease in compressive stress is mainly due to the increase of substrate temperature.

Figure 12(a) displays the influence of substrate bias voltage on the hardness and elastic modulus of TiN films deposited at a substrate temperature as low as  $10$  °C. A slight increase in hardness and elastic modulus from  $33.1$  and  $417.6$  GPa to  $35.6$  and  $430.8$  GPa was observed with increasing the substrate bias voltage from  $-50$  to  $-150$  V, and then decreased to  $32.0$  and  $396.2$  GPa with further increasing substrate bias voltage to  $-200$  V. The high hardness would be due to the small grain sizes ranging from  $6.2$  to  $13.8$  nm and high residual compressive stress ranging from  $10.2$  to  $10.7$  GPa. The increase in hardness as a function of the substrate bias voltage was correlated with the increase of compressive stress [16]. Meanwhile, the influence of substrate temperature on the hardness and elastic modulus of TiN films is shown in Fig. 12(b). The hardness and elastic modulus decreased sharply

from 33.1 and 417.6 GPa to 30.6 and 403.8 GPa with the substrate temperature increasing from 10 to 300 °C, which would be due to the fact that the effect of compressive stress plays a dominant role in the hardness of the films. It can be inferred that the relaxation of compressive stress with increasing substrate temperature could partly decrease the hardness of the films.

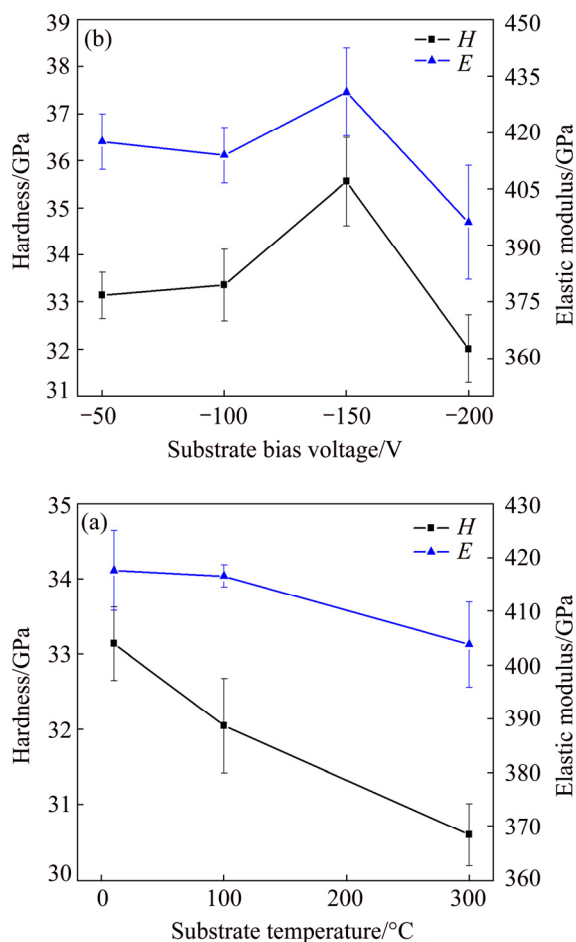


**Fig. 12** Hardness and elastic modulus of TiN films deposited at different substrate bias voltages with same substrate temperature of 10 °C (a) and at different substrate temperatures with same substrate bias voltage of -50 V (b)

The adhesive failure mode of TiN films deposited on 316L SS substrates was identified according to the scratch tracks observed by an optical microscope (OM). Generally, the peeling off stage (critical load denoted as  $L_{c2}$ ) with a rapid increase of the friction was regarded as a sign of film adhesion failure, which was defined as adhesion strength [35]. The dependence of adhesion strength on the substrate bias voltage and temperature is shown in Fig. 13. When the substrate temperature decreased to as low as 10 °C, the TiN films exhibited a low adhesion strength ranging from 6.6 to 10.5 N. The high residual compressive stress resulted in a reduction in substrate/films adhesion strength [36]. However, the

adhesion strength increased sharply from 9.9 to 21 N with the substrate temperature increasing from 10 to 300 °C, which was closely related to the residual compressive stress level in the films [37]. Moreover, it would be due to the formation of pseudo-diffusion interfaces between the substrate and film due to the higher substrate temperature [38].

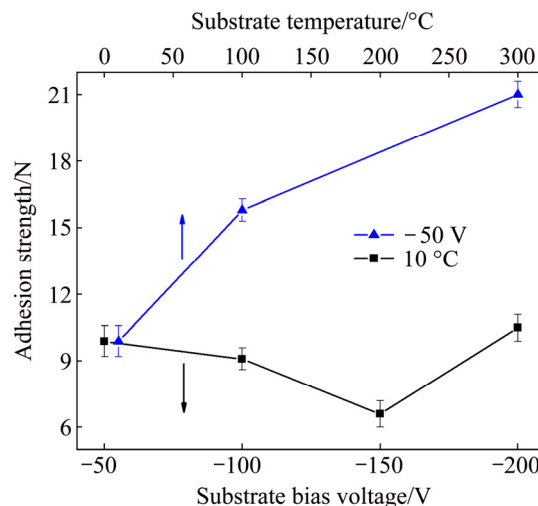


**Fig. 13** Adhesion strength of TiN films deposited at different substrate bias voltages and temperatures

## 4 Conclusions

1) As the substrate temperature increases from 10 to 300 °C, the deposition rate increases from 2.79 to 3.23  $\mu\text{m/h}$  and the diffraction peak intensity of TiN films increases gradually with simultaneous peak narrowing.

2) As the substrate temperature increases from 10 to 300 °C, the average diameter of macro-particles on the film surface increases sharply from 0.39 to 0.48  $\mu\text{m}$  and the residual compressive stress decreases sharply from 10.2 to 7.7 GPa, which leads to the hardness decreasing from 33.1 to 30.6 GPa, while the adhesion strength increases sharply from 9.6 to 21 N.

## References

- [1] LACKNER J M. Industrially-scaled large-area and high-rate tribological coating by pulsed laser deposition [J]. *Surface & Coatings Technology*, 2005, 200: 1439–1444.
- [2] AKKAN C K, MAY A, HAMMADEH M, ABDUL-KHALIQ H, AKTAS O C. Matrix shaped pulsed laser deposition: New approach to large area and homogeneous deposition [J]. *Applied Surface Science*, 2014, 302: 149–152.
- [3] KIM I, KHATKHATAY F, JIAO L, SWADENER G, COLE J I, GAN J, WANG H. TiN-based coatings on fuel cladding tubes for advanced nuclear reactors [J]. *Journal of Nuclear Materials*, 2012, 429: 143–148.
- [4] KHATKHATAY F, JIAN J, JIAO L, SU Q, GAN J, COLE J I, WANG H. Diffusion barrier properties of nitride-based coatings on fuel cladding [J]. *Journal of Alloys and Compounds*, 2013, 580: 442–448.

- [5] HONG X, TAN Y F, WANG X L, TAN H, XU T. Effects of nitrogen flux on microstructure and tribological properties of in-situ TiN coatings deposited on TC11 titanium alloy by electrospark deposition [J]. Transactions of Nonferrous Metals Society of China, 2015, 25: 3329–3338.
- [6] ZHANG M, LIN G, DONG C, WEN L. Amorphous TiO<sub>2</sub> films with high refractive index deposited by pulsed bias arc ion plating [J]. Surface & Coatings Technology, 2007, 201: 7252–7258.
- [7] ZHANG M, LI M, KIM K H, PAN F. Structural and mechanical properties of compositionally gradient CrN<sub>x</sub> coatings prepared by arc ion plating [J]. Applied Surface Science, 2009, 255: 9200–9206.
- [8] LIN S S, ZHOU K S, DAI M J, HU F, SHI Q, HOU H J, WEI C B, LI F Q, TONG X. Effects of surface roughness of substrate on properties of Ti/TiN/Zr/ZrN multilayer coatings [J]. Transactions of Nonferrous Metals Society of China, 2015, 25: 451–456.
- [9] ZHANG M, HU X G, YANG X X, XU F F, KIM K H, SHAO Z G. Influence of substrate bias on microstructure and morphology of ZrN thin films deposited by arc ion plating [J]. Transactions of Nonferrous Metals Society of China, 2012, 22(S): s115–s119.
- [10] ZHANG L, MA G J, MA H, LIN G Q. Effect of pulsed bias voltage on the structure and mechanical properties of Ti–C–N composite films by pulsed bias arc ion plating [J]. Nuclear Instruments and Methods in Physics Research B, 2014, 333: 1–5.
- [11] ZHANG M, LIU L, YANG X X, XU F F, LIU C S, GONG F Q, LI M K. Influence of pulsed bias on TiO<sub>2</sub> thin films prepared on silicon by arc ion plating: Experimental and simulation study [J]. Surface & Coatings Technology, 2013, 229: 186–190.
- [12] GUO H J, CHEN W Y, SHAN Y, WANG W Z, ZHANG Z Y, JIA J H. Microstructures and properties of titanium nitride films prepared by pulsed laser deposition at different substrate temperatures [J]. Applied Surface Science, 2015, 357: 473–478.
- [13] ZHANG D, GUAN L, LI Z, PAN G, TAN X, LI L. Simulation of island aggregation influenced by substrate temperature, incidence kinetic energy and intensity in pulsed laser deposition [J]. Applied Surface Science, 2006, 253: 874–880.
- [14] PANDEY S K, THAKUR O P, RAMAN R, GOYAL A, GUPTA A. Structural and optical properties of YSZ thin films grown by PLD technique [J]. Applied Surface Science, 2011, 257: 6833–6836.
- [15] FESSMANN J, OLBRICH W, KAMPSCHULTE G, EBBERINK J. Cathodic arc deposition of TiN and Zr(C, N) at low substrate temperature using a pulsed bias voltage [J]. Materials Science and Engineering A, 1991, 140: 830–837.
- [16] MEDJANI F, SANJINÉS R, ALLIDI G, KARIMI A. Effect of substrate temperature and bias voltage on the crystallite orientation in RF magnetron sputtered AlN thin films [J]. Thin Solid Films, 2006, 515: 260–265.
- [17] WANG Q M, KIM K H. Effect of negative bias voltage on CrN films deposited by arc ion plating. I. Macroparticles filtration and film-growth characteristics [J]. Journal of Vacuum Science & Technology A, 2008, 26: 1258–1266.
- [18] STONEY G G. The tension of metallic films deposited by electrolysis [J]. Proceedings of the Royal Society A, 1909, 82: 172–175.
- [19] WAN X S, ZHAO S S, YANG Y, GONG J, SUN C. Effects of nitrogen pressure and pulse bias voltage on the properties of Cr–N coatings deposited by arc ion plating [J]. Surface & Coatings Technology, 2010, 204: 1800–1810.
- [20] GHIMBEU C M, SIMA F, OSTACI R V, SOCOL G, MIHAILESCU I N, VIX-GUTERL C. Crystalline vanadium nitride ultra-thin films obtained at room temperature by pulsed laser deposition [J]. Surface & Coatings Technology, 2012, 211: 158–162.
- [21] KHAN S, MEHMOOD M, SAEED S, KHAN T M, SADIQ G, AHMED I. Effect of substrate biasing and temperature on AlN thin film deposited by cathodic arc ion [J]. Materials Science in Semiconductor Processing, 2013, 16: 640–646.
- [22] KRZANOWSKI J E, PHANI A R. Preferential growth of Ti and TiN films on Si (111) deposited by pulsed laser deposition [J]. Applied Surface Science, 2001, 174: 132–137.
- [23] PARK I W, KANG D S, MOORE J J, KWON S C, RHA J J, KIM K H. Microstructures, mechanical properties, and tribological behaviors of Cr–Al–N, Cr–Si–N, and Cr–Al–Si–N coatings by a hybrid coating system [J]. Surface & Coatings Technology, 2007, 201: 5223–5227.
- [24] WANG Q M, KIM K H. Microstructural control of Cr–Si–N films by a hybrid arc ion plating and magnetron sputtering process [J]. Acta Materialia, 2009, 57: 4974–4987.
- [25] SPANIER J E, ROBINSON R D, ZHANG F, CHAN S W, HERMAN I P. Size-dependent properties of CeO<sub>2-x</sub> nanoparticles as studied by Raman scattering [J]. Physical Review B, 2001, 64: 245–407.
- [26] BANERJEE R, CHANDRA R, AYYUB P. Influence of the sputtering gas on the preferred orientation of nanocrystalline titanium nitride thin films [J]. Thin Solid Films, 2002, 405: 64–72.
- [27] ZHANG S H, WANG L, WANG Q M, LI M X. A superhard CrAlSiN superlattice coating deposited by multi-arc ion plating: I. Microstructure and mechanical properties [J]. Surface & Coatings Technology, 2013, 214: 160–167.
- [28] ZHANG G P, GAO G J, WANG X Q, LV G H, ZHOU L, CHEN H, PANG H, YANG S Z. Influence of pulsed substrate bias on the structure and properties of Ti–Al–N films deposited by cathodic vacuum arc [J]. Applied Surface Science, 2012, 258: 7274–7279.
- [29] WANG Y J, LI H X, JI L, ZHAO F, KONG Q H, WANG Y X, LIU X H, QUAN W L, ZHOU H D, CHEN J M. Microstructure, mechanical and tribological properties of graphite-like amorphous carbon films prepared by unbalanced magnetron sputtering [J]. Surface & Coatings Technology, 2011, 205: 3058–3065.
- [30] MUSIL J, POULEK V, VALVODA V, KUŽEL R, JEHN H A, BAUMGÄTNER M E. Relation of deposition conditions of Ti–N films prepared by dc magnetron sputtering to their microstructure and macrostress [J]. Surface & Coatings Technology, 1993, 60: 484–488.
- [31] D'HEURLE F M, HARPER J M E. Note on the origin of intrinsic stresses in films deposited via evaporation and sputtering [J]. Thin Solid Films, 1989, 171: 81–92.
- [32] KHAMSEH S, NOSE M, KAWABATA T, NAGAE T, MATSUDA K, IKENO S. A comparative study of CrAlN films synthesized by dc and pulsed dc reactive magnetron facing target sputtering system with different pulse frequencies [J]. Journal of Alloys and Compounds, 2010, 508: 191–195.
- [33] LIU G, YANG Y Q, HUANG B, LUO X, OUYANG S, ZHAO G M, JIN N, LI P T. Effects of substrate temperature on the structure, residual stress and nanohardness of Ti6Al4V films prepared by magnetron sputtering [J]. Applied Surface Science, 2016, 370: 53–58.
- [34] ZHANG L Q, YANG H S, PANG X L, GAO K W, VOLINSKY A A. Microstructure, residual stress, and fracture of sputtered TiN films [J]. Surface & Coatings Technology, 2013, 224: 120–125.
- [35] WANG L, ZHANG S H, CHEN Z, LI J L, LI M X. Influence of deposition parameters on hard Cr–Al–N coatings deposited by multi-arc ion plating [J]. Applied Surface Science, 2012, 258: 3629–3636.
- [36] BULL S J, RICKERBY D S. The inter-relationship between coating microstructure and the tribological performance of PVD coatings [C]//Mechanics of Coatings. Amsterdam: Elsevier Science B. V., 1990: 337–349.
- [37] STALLARD J, POULAT S, TEER D G. The study of the adhesion of a TiN coating on steel and titanium alloy substrates using a multi-mode scratch tester [J]. Tribology International, 2006, 39: 159–166.
- [38] ZHANG D, GUAN L, LI Z, PAN G, TAN X, LI L. Simulation of island aggregation influenced by substrate temperature, incidence kinetic energy and intensity in pulsed laser deposition [J]. Applied Surface Science, 2006, 253: 874–880.

## 电弧离子镀低温沉积 TiN 薄膜的 显微结构与残余应力

梅海娟<sup>1,2</sup>, 赵升升<sup>1</sup>, 陈伟<sup>1</sup>, 王启民<sup>2</sup>, 梁海峰<sup>3</sup>

1. 深圳职业技术学院 机电工程学院, 深圳 518055;

2. 广东工业大学 机电工程学院, 广州 510006;

3. 华东交通大学 理工学院, 南昌 330100

**摘要:** 采用电弧离子镀技术在 316L 不锈钢基体上低温沉积 TiN 薄膜, 并利用 EDS、SEM、XRD 和纳米压痕仪研究基体偏压和温度对薄膜的显微结构、残余应力和力学性能的影响规律。结果表明, TiN 薄膜表现出高度(111)择优取向的面心立方结构。随着基体偏压和温度的增加, 衍射峰强度急剧增加, 同时峰变窄, 晶粒尺寸从 6.2 nm 增大到 13.8 nm。当基体温度从 10 °C 增加到 300 °C 时, 薄膜的残余压应力从 10.2 GPa 急剧下降到 7.7 GPa, 从而导致薄膜的硬度从 33.1 GPa 下降到 30.6 GPa, 而薄膜的结合力则从 9.6 N 增加到 21 N。

**关键词:** TiN 薄膜; 电弧离子镀; 残余应力; 低温; 偏压

(Edited by Xiang-qun LI)